Electrochimica Acta 153 (2015) 300–305

Contents lists available at ScienceDirect

Electrochimica Acta

journal homepage: www.elsevier.com/locate/electacta

Fe-added Fe_3C carbon nanofibers as anode for Li ion batteries with excellent low-temperature performance

Jiaxin Li [a,b], Weiwei Wen [b], Guigui Xu [b], Mingzhong Zou [b], Zhigao Huang [b], Lunhui Guan [a,c,*]

[a] State Key Laboratory of Structural Chemistry, Fujian Institute of Research on the Structure of Matter, Chinese Academy of Sciences, Fuzhou 350002, China
[b] College of Physics and Energy, Fujian Normal University, Fuzhou, 350007, China
[c] Key Laboratory of Design and Assembly of Functional Nanostructures, Chinese Academy of Sciences, Fuzhou, 350002, China

ARTICLE INFO

Article history:
Received 11 October 2014
Received in revised form 20 November 2014
Accepted 2 December 2014
Available online 3 December 2014

Keywords:
Lithium batteries
Fe/Fe_3C—CNF anodes
Low-temperature performance
Electrospinning

ABSTRACT

The poor conductivity of anodic carbon materials at low temperature hampers their high-level applications in Li ion batteries (LIBs). Introducing some reliable metals with good electrical conductivity into anodes could alleviate these problems. In this work, the novel composites of Fe-added Fe_3C carbon nanofibers (Fe/Fe_3C—CNFs) were synthesized *via* facile electrospinning method and used as anode materials for LIBs. The resulting anodes with Fe/Fe_3C—CNF materials exhibited a high reversible capacity of 500 mAh g^{-1} tested at 200 mA g^{-1} even after 70 cycles and excellent performance at room temperature. Importantly, it delivered a high capacity of 250 mAh g^{-1} at 400 mA g^{-1} even after 55 cycles at a low temperature of −15 °C. The superior low-temperature electrochemical performance of the Fe/Fe_3C—CNF anodes is associated with an improved effect of the highly conducting Fe at low temperature.

1. Introduction

Increasing energy demands of portable electronic devices and hybrid electric vehicles have stimulated extensive research on high-performance Li ion batteries (LIBs) [1,2]. Over the past decade, enormous efforts have been devoted to explore various LIB anodic materials, especially for graphite and modified carbon-based materials [2–4]. However, exploring high-performance anodic materials especially at low temperature is still too lack to meet the increasingly growing demand [5–7]. Usually, the conductivity attenuation combined with substantial microstructure change at low temperature, resulting in large interface polarization and performance deterioration, hampers their high-level applications in LIBs [8,9]. Typically for carbon-based materials, the reduced ability of carbonaceous materials to intercalate lithium into their structures at low temperatures would be also deteriorated, which may be attributed to the increasing charge-transfer resistance with decreasing temperature.

To mitigate the detrimental effects of conductivity attenuation, several strategies have been recently reported, including the utilization of metal nanoparticles (NPs) attached on the surface of anode materials and the utilization of metal layer covered on the materials [9–12]. As a typical example, *Huang*'s group has reported that anode of Ag-incorporated Fe_2O_3 carbon nanofibers (CNFs) exhibit an obvious enhanced low-temperature electrochemical performance [9]. It is believed that those Ag NPs possess better conductivity at low temperature than that at room temperature, thereby significantly improving their electrochemical performance at low temperature. For the price consideration, to use some cheap reliable metals such as Fe and Cu also with good electrical conductivity instead of Ag is important for potential practical LIBs. Thus, to develop an effective method to fabricate anode composites with highly dispersed cheap metal NPs and excellent conductivity is desired.

In addition to the strategies on the improvement of conductivity, the development of high-capacity carbon materials is also strongly needed. Recently, Zhou et al. certifed that introducing nano-sized metal catalyst for carbon anodic materials can reduce some SEI components and further improve the reversible capacities for carbon anodes [13,14]. As expected, it is reported that Ni/C hierarchical composites, which consist of Ni nanoparticles highly dispersed in N-containing carbon nanosheets, can afford an unexpected reversible capacity of 1051 mAh g^{-1} after 30 cycles and 635 mAh g^{-1} after 100 cycles at the current density of 200 mA g^{-1} [14]. Especially, iron carbide (Fe_3C), with high catalytic activity, extreme hardness and sufficient thermal stability, has attracted interests of researchers in LIBs [15,16]. For example, the Fe_3C/C composite showed a stable discharge capacity of 750 mAh

* Corresponding author. Tel.: +86 591 83792835; fax: +86 591 83792835.
E-mail address: guanlh@fjirsm.ac.cn (L. Guan).

http://dx.doi.org/10.1016/j.electacta.2014.12.008
0013-4686/

g^{-1} after 120 cycles at 1000 mA g^{-1}, which values are much larger than pure carbon electrodes [17]. Some recent reports suggest that Fe_3C can reduce some SEI components and further improve the reversible capacities for carbon anodes [16,18]. Besides, it is generally recognized that CNFs with unique structure, large aspect ratio, and favorable flexibility have been proven to be good candidates for carbon anodes [19]. Thus, to explore whether the Fe_3C material can enhance the capacity of CNFs is also interesting and desired.

In this work, we attempt to introduce cheap reliable iron metal to uniformly add in the composite of Fe_3C CNFs via a simple in-situ electrospinning method (shown in Scheme 1) and form a homogeneous hybrid material of Fe/Fe_3C—CNFs, with the aim of improving its electrochemical performance for LIBs especially at low temperature. Compared with the pure CNFs, Fe/Fe_3C—CNF anodes exhibited obviously better low-temperature electrochemical performance including reversible capacity, cycling performance, and rate performance.

2. Experimental Part

2.1. Materials synthesis

In this work, all chemicals were of analytical grade and used as received. The samples were all prepared by an electrospinning method based on our previous study [20]. Typically, 2.5 g of polyacrylonitrile (PAN, *Mw* about 150000) was dissolved in 25 ml of N, N-dimethylformamide (DMF), and then 4.5 g of $FeC_2O_4{\cdot}2H_2O$ were added to form a mixed solution. After vigorous stirring for 40 h at 60 °C, a sticky sol was obtained. A high voltage power supply was used to provide a 15 kV high voltage for the as-prepared electrospinning solutions. The feed speed rate and needle-to-collector distance were set up at 0.8 ml h^{-1} and 15 cm, respectively. The nanofibers were collected on a self-manufactured collector, and then dried for 24 h in vacuum at 80 °C. The dried nanofibers were further stabilized in air at 260 °C for 3 h with a heating rate of 2 °C min^{-1}. Finally, the stabilized nanofibers were annealed in a Ar flow at 550 °C for 1 h with a heating rate of 2 °C min^{-1} for forming Fe/Fe_3C—CNF composite. The process is briefly shown in Scheme 1. For comparison, the different consumption of $FeC_2O_4{\cdot}2H_2O$ precursor used in the experiments were investigated. Herein, we added $FeC_2O_4{\cdot}2H_2O$ with different contents of 2.0, 4.5 and 7.5 g to the same solution, and the products were symbolized as sample1 to sample3, respectively. Herein, the electrodes used in the following manuscript were prepared by using sample2 without additional illustration, while the result of sample1 and sample3 were presented in the Electronic Supplementary Material.

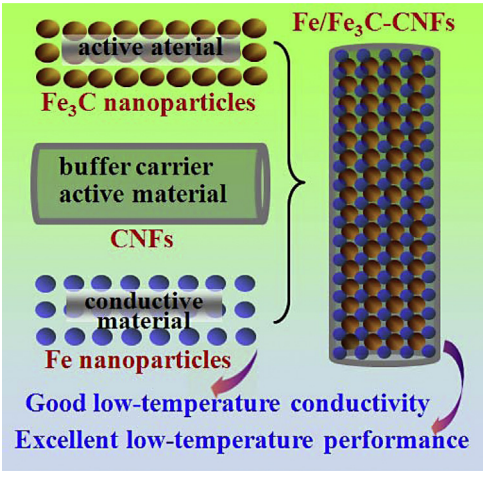

Scheme 1. Schematic illustration of the fabrication of Fe/Fe_3C—CNFs.

2.2. Materials Characterization

The structure and morphology of the samples were characterized by X-ray diffraction (XRD, RIGAKU SCXmini), energy dispersive X-ray spectroscopy (EDS), X-ray Photoelectron Spectroscopy, scanning electron microscope (SEM, JSM-6700F), transmission electron microscope (TEM, Tecnai G2 F20), thermal gravimetric analysis (TGA,NETZSCH STA449C) and X-ray Photoelectron Spectroscopy (XPS, ESCALAB 250).

2.3. Electrochemical measurements

The electrochemical behaviors were measured via CR2025 coin-type test cells assembled in a dry argon-filled glove box. The test cell consisted of working electrode (~1.5 mg cm^{-2}) and lithium sheet which were separated by a Celgard 2300 membrane and electrolyte of 1 M LiPF6 in EC:EMC:DMC (1:1:1 in volume). The working electrode consisted of 80 *wt.* % active material, 10 *wt.* % carbon black and 10 *wt.* % polymer binder (Carboxymethyl cellulose, Na-CMC). The electrodes were dried at 100 °C for 12 h in a vacuum. Cyclic voltammetry tests were operated on a CHI660D Electrochemical Workstation with a scan rate of 0.50 mV s^{-1}. The cells were cycled by LAND 2001 A at room temperature. Electrochemical impedance measurements were carried out by applying an ac voltage of 5 mV over the frequency range from 1 mHz to 100 kHz.

3. Results and discussion

As shown in the Fig. 1, the morphology and structure of the Fe/Fe_3C—CNFs were examined by SEM, XRD, TEM and HR-TEM. From Fig. 1a, SEM image reveals that Fe/Fe_3C—CNFs are consisted of randomly oriented, overlapped, continuous and interconnected nanofibers. The diameter for these nanofibers is ranging from 300 to 450 nm. The XRD analyses illustrated in Fig. 1b indicate that metallic Fe, Fe_3C and graphitic carbon coexisted, according to the diffraction data for α-Fe (JCPDS No. 87-0722) and Fe_3C (JCPDS No. 89-2867) [21]. Meanwhile, the EDS result shown in Fig. S1 provides another proof of Fe element in the obtained CNFs. For revealing the possible formation mechanism of Fe/Fe_3C, the different consumption of $FeC_2O_4{\bullet}2H_2O$ precursor used in the experiments were investigated. The related XRD and TGA results have been display in Figs. S2 and S3. The TEM, HR-TEM and the corresponding SAED analysis of Fe/Fe_3C—CNFs are shown in Fig. 1c~d. The Fig. 1c reveals the interplanar spacing of 0.20 and 0.30 nm, corresponding to the Fe(110) and Fe_3C (111) planes, respectively. The corresponding SAED pattern provided in the inset of Fig. 1d also confirms the formation of crystalline nature of Fe/Fe_3C—CNFs. The diffraction rings are related to the (111) and (121) planes for Fe_3C, (110) and (200) planes for metallic Fe. Other detailed HR-TEM images are presented in the Fig. S4.

Additionally, the Fig. 2 shows the XPS spectra of pure CNFs and Fe/Fe_3C—CNFs. As revealed in the O1s XPS spectra in Fig. 2f, iron oxides are lightly detected at 529.5 eV. Meanwhile, two peaks of the O1s spectra for both CNFs and Fe/Fe_3C—CNFs shown in Fig. 2b and f are similar, further revealing little iron oxides in the obtained composites may due to the oxidation of the trace amounts of Fe in the surface. From the Fe2p XPS spectra (Fig. 2g) it is evident that metallic iron (Fe^0) at 707.1 eV and Fe_3C at 708.2 eV are present in the as-prepared composites. The Fe 2p3/2 peaks at 724.2, 719.8 and 710.8 eV are unique peaks for ferric irons, which result is consistent with the O1s spectra. Furthermore, in the comparison of C1S for pure CNFs and Fe/Fe_3C—CNFs shown Fig. 2d and h, a typical

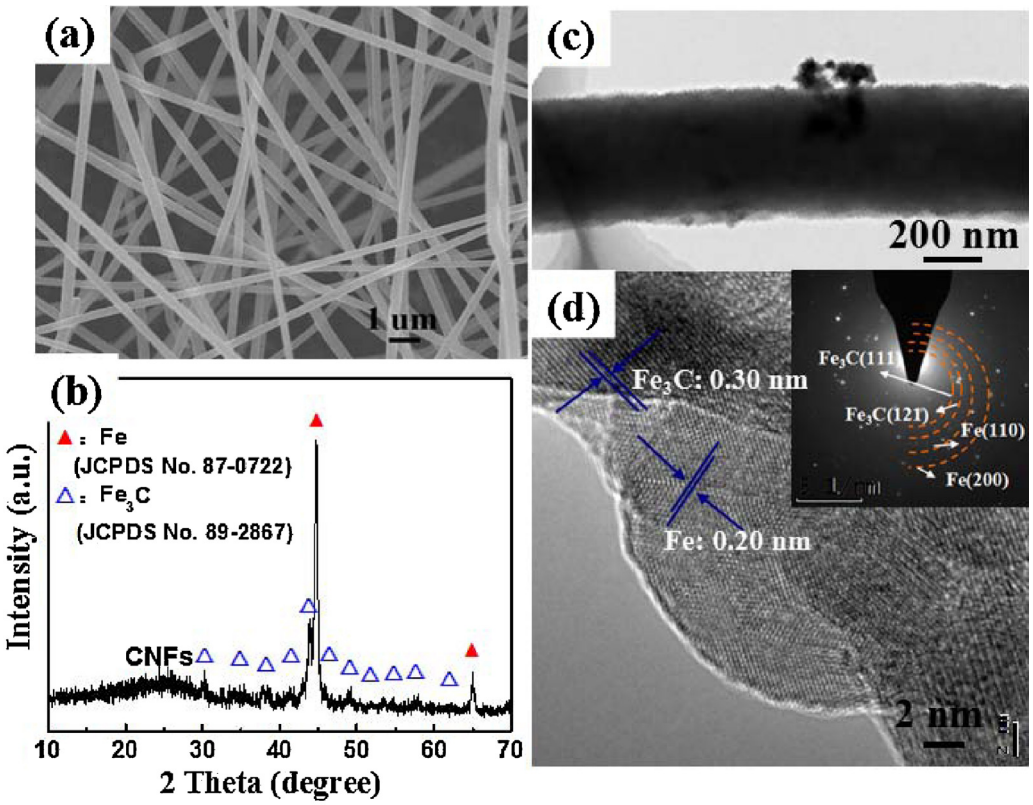

Fig. 1. (a) SEM image of Fe/Fe_3C-CNFs; (b) XRD pattern of Fe/Fe_3C—CNFs; (c) TEM image of Fe/Fe_3C—CNFs; (d) the HR-TEM image and SAED pattern of Fe/Fe_3C—CNFs.

sp2C—C peak at 284.5 eV along with a sp3C=C peak at 285.2 eV indicated in both samples are from the carbon layers in CNFs, and the appearance of broaden C—Fe bonding at 283.5 eV in the Fe/Fe_3C—CNF sample can be attributed to the formation of Fe_3C. Anyhow, combined with the XRD analysis in the manuscript, these results indicate that most iron species exist as metallic Fe or iron carbide (Fe_3C), with little iron oxide on the surface.

The electrochemical performance of the CNFs and Fe/Fe_3C—CNFs used for LIBs at 25 °C is investigated. From Fig. 3a, the first discharge/charge (D/C) curves of CNF electrode deliver capacities of 878 and 421 mAh g^{-1}, implying an irreversible capacity loss of ~52.1%. In contrast, the first D/C capacities for the Fe/Fe_3C—CNF electrode were 961 and 525 mAh g^{-1}, with a smaller loss of ~45.4% compared with the CNFs. In addition, the first two D/C curves of

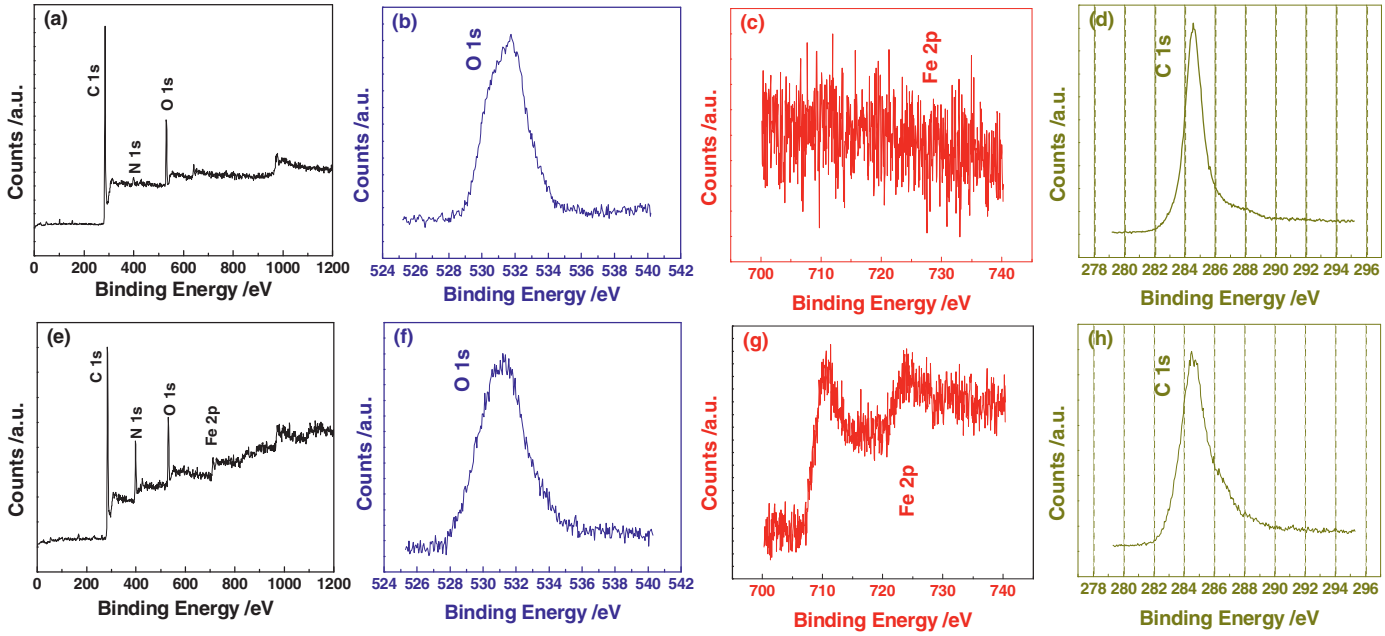

Fig. 2. XPS spectra for (a,b) CNFs and (c–e) Fe/Fe_3C—CNFs.

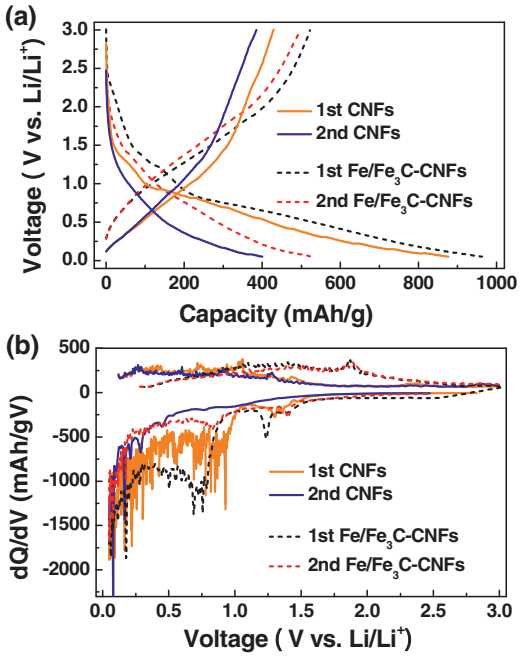

Fig. 3. (a) Discharge/charge voltage profiles of the CNFs and Fe/Fe_3C—CNFs, respectively; (b) differential capacity versus voltage plots of the CNFs and Fe/Fe_3C—CNFs corresponding to the first two cycles.

Fe/Fe_3C—CNFs are quite different from the pure CNFs. To better illustrate the redox reactions, differential capacity versus voltage (dQ/dV) curves of the first two cycles are investigated in Fig. 3b. Upon discharge, the broad peak at ~0.8 V (solid line for pure CNF anode) is observed, corresponding to the starting formation of SEI films. This peak greatly decreased during the subsequent cycle, which was attributed to the irreversible formation of SEI components. The following peak from 0.4 to 0.05 V is attributed to the Li insert to the pure CNFs. Conversely, for the Fe/Fe_3C—CNFs, two reduction peaks (dotted line for pure Fe/Fe_3C—CNF anode) are found at 1.3 and 0.9 V in the 1st cycle, and they appear in the 2nd cycle which can be assigned to the formation of reversible SEI films and the additional sites for Li intercalation. Besides, a broad oxidation peak located from 1.2 to 2.0 V is related to the Li extraction from SEI films and the partial polarization effect [16,18]. It is one of the reasons for the great capacity difference between the CNF and Fe/Fe_3C—CNF anodes. The redox peaks of both of CNFs and Fe/Fe_3C—CNFs in the 2nd cycle overlap well with those in the 1st cycle, indicating their better electrochemical reversibility and structural stability.

Furthermore, the cyclic voltammetry test for Fe/Fe_3C—CNFs revealed the similar mechanism compared with the dQ/dV curves.

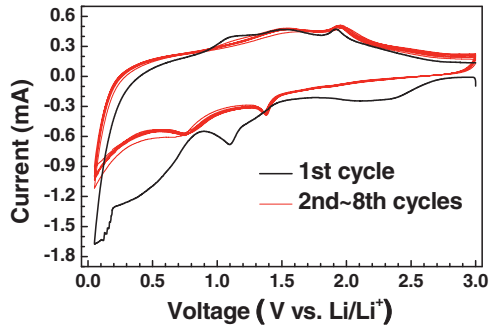

Fig. 4. Cyclic voltammetry curves between 0.05 and 3 V of Li insertion/extraction into/from the of Fe/Fe_3C-CNF anode at room temperature of 25 °C.

Fig. 4 shows the cyclic voltammetry curves between 0.05 and 3 V of Li insertion/extraction into/from the of Fe/Fe_3C—CNF anode at room temperature of 25 °C. Being different from the normal CNF-based anodes [8,19], an additional huge peak appears at 0.4–1.0 V in the initial discharge curve. According to the previous report [13], this peak cannot be assigned to the reduction of Fe^{3+} and Fe^{2+}. Instead, it should belong to the main formation of the SEI films. Thus, an obvious and broad oxidation peak (1.1~2.0 V) demonstrates the preliminary decomposition of SEI. These additional redox peaks can afford enhanced Li ion insertion/extraction for the Fe/Fe_3C—CNF anode. The redox peaks at the 2nd-8th cycles almost overlap with each other, also indicating the reversible oxidation of some SEI components and good cycling stability.

Fig. 5a and b compared the cycling performance of CNFs and Fe/Fe_3C—CNFs. The Fe/Fe_3C—CNF anodes exhibit much better cyclic stability and rate performance than those of the bare CNF anodes. It is also observed that the reversible capacity of Fe/Fe_3C—CNFs remained at ~500 mAh g^{-1} tested at 200 mA g^{-1} after 70 cycles, while that of only 230 mAh g^{-1} for the pure CNFs. As revealed by the TGA result shown in the Fig. S3, the mass contents of Fe/Fe_3C and CNFs in the sample2 of Fe/Fe_3C—CNFs are ~34wt% and ~63wt %, respectively. Thus, subtracting the contribution from the CNFs in Fe/Fe_3C—CNF composite, a reversible capacity about 1040 mAh/g can be attributed to the additional capacities from SEI film, indicating the good catalysitic effect from Fe_3C. For approximate processing, the calculated capacity of 1040 mAh/g is based on the following equation: $[C_{Fe/Fe3C-CNFs} - (C_{CNFs} \times 63\ wt.\%)]/34\ wt.\% = [500 - (232 \times 0.63)]/0.34 = 1040$. The good catalysitic effect can effectively facilitate the high electrochemical performance of the Fe/Fe_3C—CNF electrodes. Furthermore, Fig. S5 shows the TEM image and the corresponding SAED for Fe/Fe_3C—CNFs after cycling. The good morphology retention after electrochemical testing can effectively facilitate the high stability of the Fe/Fe_3C—CNFs.

It is previously reported that the charge-transfer resistance for carbonaceous materials would increase obviously with decreasing the temperature [6,7,9]. However, the case of metal Fe is contrast from the carbonaceous materials. Therefore, exploring the Fe/Fe_3C—CNF anodes especially at low temperatures should be

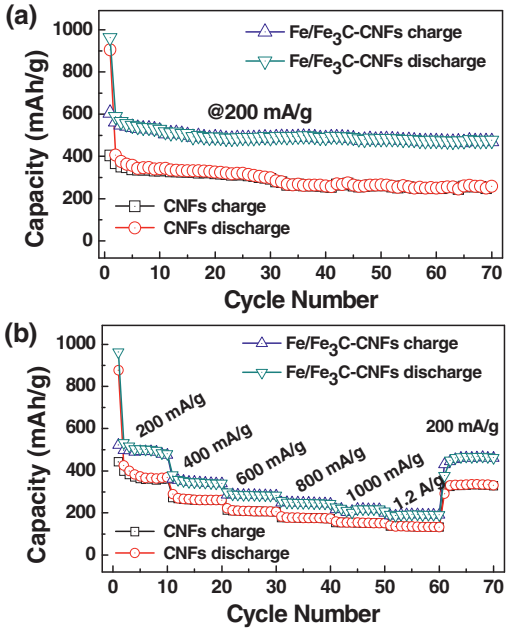

Fig. 5. Comparative cycling performance of the (a) CNFs and (b) Fe/Fe_3C—CNFs. All the tests were taken between 0.05 and 3.0 V at room temperature of 25 °C.

interesting and desired. Fig. 6a and b show the electrochemical performances of the CNFs and Fe/Fe_3C—CNFs under low temperatures of 5 and −15 °C at different current densities of 200 mA g^{-1} and 400 mA g^{-1}, respectively. All the cycle performance is obtained after being activated at 200 mA g^{-1} in the first three cycles. As expected, the Fe/Fe_3C—CNF anodes exhibit much larger reversible capacities and better cyclic stability than the bare CNF anodes at different temperatures of both of 5 and −15 °C. After 40 cycles, the CNF anode delivers a specific reversible capacity of 90 mAh g^{-1} tested at 5 °C (Fig. 6a). In comparison, a lager specific reversible capacity for Fe/Fe_3C—CNFs stabilized at 400 mAh g^{-1}. Furthermore, when the cells were tested at a lower temperature of −15 °C (Fig. 6b), the reversible capacities of CNFs and Fe/Fe_3C—CNFs remained at ~20 and ~270 mAh g^{-1} tested at 400 mA g^{-1} after 40 cycles. Interestingly, the reversible capacities for these two samples decreased with decreasing the tested temperature. To clearly compare the electrochemical performance of these two anodes, the reversible capacities of CNFs and Fe/Fe_3C—CNFs after 50 cycles tested at 200 mA g^{-1} versus the different temperatures of 25, 5 and −15 °C has been summarized in Table 1. The Fe/Fe_3C—CNFs can deliver capacities of 500, 420 and 380 mAh g^{-1} at 25, 5 and −15 °C respectively, resulting in a capacity loss of ~24% (i.e., (500 − 380)/500 = 24%). By contrast, with the decrease of tested temperature, the CNF anode shows a much larger capacity loss of ~65% (i.e., (230 − 80)/230 = 65%). For further evaluating the enhanced effect of Fe incorporating on the improved performance for Fe_3C—CNFs, the Fe/Fe_3C—CNFs consisted of massive Fe_3C (signed as sample 1 in the ESI) have been prepared and used to investigate as LIB anodes. Compared with the Fe/Fe_3C—CNFs shown in the Figs. 5 and 6, the cycling performance of sample 1 presented in the Fig. S6 exhibits an obviously worse LIB performance including cyclic stability and rate performance, especially for the low-temperature performance.

Table 1
The comparison of the reversible capacities of CNFs and Fe/Fe_3C—CNFs after 50 cycles tested at 200 mA g^{-1} versus the different temperatures.

Temperature/°C	Capacities/mAh g^{-1} for Fe/Fe_3 C—CNFs	Capacities/mAh g^{-1} for CNFs
25	500	230
5	420	200
−15	380	80

The improved performance should be caused by the enhanced conductivity and unique architecture of Fe/Fe_3C—CNFs. As revealed in Fig. 7a and b, the difference of total resistance between CNFs and Fe/Fe_3C—CNFs tested at 5 °C are several hundreds of Ohm. Most importantly, this difference increased sharply to several thousands of Ohm when the temperature was reduced to −15 °C, demonstrating a more deteriorated resistance for pure CNFs tested at a lower temperature. Besides, from the Fig. S7, the EIS result also reveals that the conductivity for these two samples tested at 25 °C are similar. These results indicated that the presence of Fe incorporating can significantly improve the conductivity and charge transfer resistance for electrodes especially at a low temperature, and further enhance the LIB performance. In addition, the electrochemical performance for the batteries in practical application was usually carried out under direct-current mode. Thus, according to scattering theory of electron transport across the interface, the improvement of the conductivity in electrode can result in a low interface polarization, which is considered to be responsible for the enhancement of the electrochemical performance [8]. The preliminary result manifests that this method is promising for high-performance LIBs especially at low temperature.

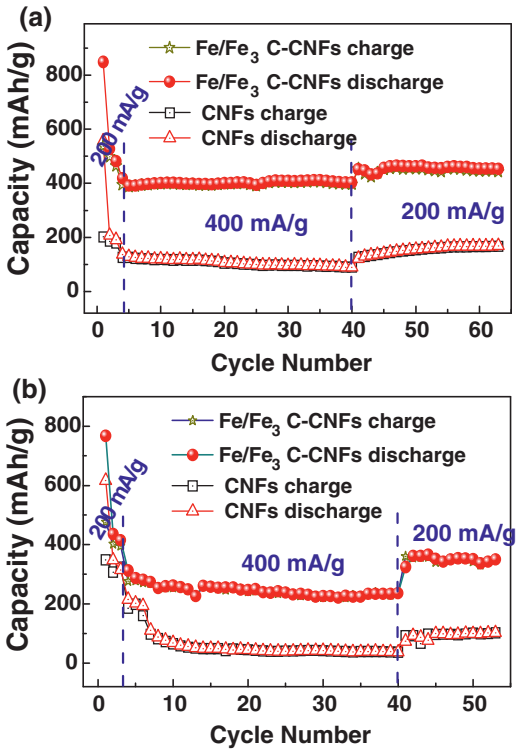

Fig. 6. The comparative cycling performance of the CNFs and Fe/Fe_3C CNFs: (a) 5 °C and (b) −15 °C.

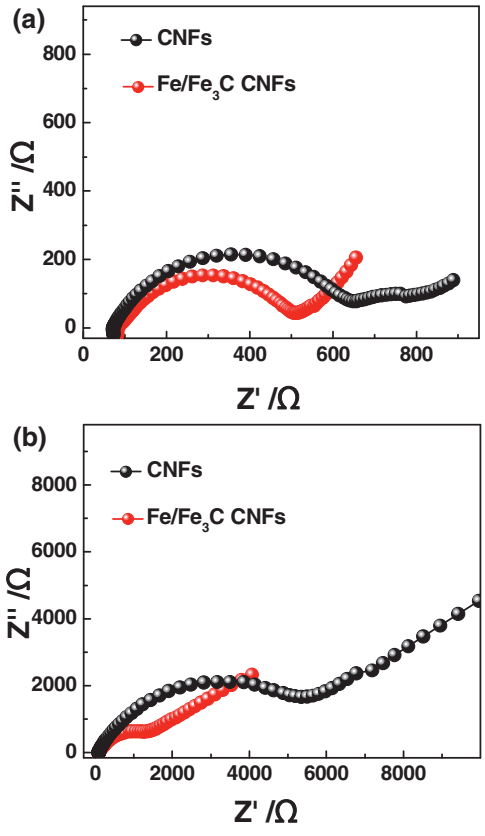

Fig. 7. The comparative electrochemical impedance spectra for CNF and Fe/Fe_3C—CNF electrodes after long electrochemical tested at (a) 5 °C and (b) −15 °C.

4. Conclusions

In summary, the novel composites of Fe/Fe_3C-CNFs prepared via a simple electrospinning method were used as anodes for LIBs. Benefiting from the synergistic effect of the fast kinetics of electron transport provided by the Fe incorporating, the Fe/Fe_3C—CNF anodes displayed a high capacity, excellent rate performance and superior low-temperature performance. The Fe/Fe_3C—CNFs delivered a high capacity of 250 mAh g^{-1} at 400 mA g^{-1} even after 55 cycles at a low temperature of −15 °C. This preliminary work provides a useful strategy to synthesize high performance LIB anode materials for use in high-level applications.

Acknowledgements

We acknowledge the financial support by the Natural Science Foundations of China (No. 21203025,11204038), the Strategic Priority Research Program of the Chinese Academy of Sciences (Grant No. XDA09010400).

Appendix A. Supplementary data

Supplementary data associated with this article can be found, in the online version, at http://dx.doi.org/10.1016/j.electacta.2014.12.008.

References

[1] B. Lim, J. Jin, J. Yoo, S.Y. Han, K. Kim, S. Kang, N. Park, S.M. Lee, H.J. Kim, S.U. Son, Chemical Communications 50 (2014) 7723–7726.
[2] M.V. Reddy, G.V. Subba Rao, B.V. Chowdari, Chemical reviews 113 (2013) 5364–5467.
[3] H.S. Jadhav, R.S. Kalubarme, C.N. Park, J. Kim, C.J. Park, Nanoscale 6 (2014) 10071–10076.
[4] S. Wang, Y. Ren, G. Liu, Y. Xing, S. Zhang, Nanoscale 6 (2014) 3508–3512.
[5] M. Marinaroa, M. Pfanzelt, P. Kubiak, R. Marassi, M. Mehrens, Journal of Power Sources 196 (2011) 9825–9829.
[6] H. Cho, W. Choi, J. Go, S. Bae, H. Shin, Journal of Power Sources 198 (2012) 273–280.
[7] F. Teng, Z. Hu, X. Ma, L. Zhang, C. Ding, Y. Yu, C. Chen, Electrochimica Acta 91 (2013) 43–49.
[8] J. Li, M. Zou, Y. Zhao, Y. Lin, H. Lai, L. Guan, Z. Huang, Electrochimica Acta 111 (2013) 165–171.
[9] M. Zou, J. Li, W. Wen, L. Chen, L. Guan, H. Lai, Z. Huang, Journal of Power Sources 46 (2014) 468–474.
[10] M. Mancini, F. Nobili, S. Dsoke, F. Amico, R. Tossici, F. Croce, R. Marassi, Journal of Power Sources 190 (2009) 141–148.
[11] F. Nobili, M. Mancini, S. Dsoke, R. Tossici, R. Marassi, Journal of Power Sources 195 (2010) 7090–7097.
[12] M. Marinaro, F. Nobili, A. Birrozzi, S. Moorthy, U. Kaiser, R. Tossici, R. Marassia, Electrochimica Acta 109 (2013) 207–213.
[13] L. Su, Y. Zhong, Z. Zhou, Journal of Materals Chemistry A 1 (2013) 15158–15166.
[14] L. Su, Z. Zhou, P. Shen, The Journal of Physical Chemistry C 116 (2012) 23974–23980.
[15] J.-S. Lee, G.S. Park, S.T. Kim, M. Liu, J. Cho, Angewandte Chemie 125 (2013) 1060–1063.
[16] Y. Tan, K. Zhu, D. Li, F. Bai, Y. Wei, P. Zhang, Chemical Engineering Journal 258 (2014) 93–100.
[17] X. Zhao, D. Xia, J. Yue, S. Liu, Electrochimica Acta 116 (2014) 292–299.
[18] L. Su, Z. Zhou, P. Shen, Electrochimica Acta 87 (2013) 180–185.
[19] J. Li, M. Zou, Y. Zhao, Z. Huang, L. Guan, RSC Advances 3 (2013) (1925) 1–19254.
[20] J. Li, M. Zou, L. Chen, Z. Huang, L. Guan, Journal of Materials Chemistry A 2 (2014) 10634–10638.
[21] Z. Wen, S. Ci, F. Zhang, X. Feng, S. Cui, S. Mao, S. Luo, Z. He, J. Chen, Adv Mater 24 (2012) 1399–1402.